Chemical Science

EDGE ARTICLE

View Article Online
View Journal | View Issue

Cite this: *Chem. Sci.*, 2015, **6**, 2187

Interconvertible multiple photoluminescence color of a gold(I) isocyanide complex in the solid state: solvent-induced blue-shifted and mechano-responsive red-shifted photoluminescence†

Tomohiro Seki,[a] Taichi Ozaki,[a] Takuma Okura,[a] Kiyotaka Asakura,[b] Aya Sakon,[c] Hidehiro Uekusa*[c] and Hajime Ito*[a]

In this study, we report the interconvertible tetracolored solid state photoluminescence of gold(I) isocyanide complex **2** upon various external stimuli through solid state structural changes. Soaking complex **2** in acetone yields blue emission as a result of the formation of **2B**. The subsequent removal of acetone yields **2G** through a crystal-to-crystal phase transition, which exhibits green emission. This green-emitting solid **2G** exhibits stepwise emission color changes to yellow and then to orange upon mechanical stimulation by ball-milling, which corresponds to the formation of **2Y** and **2O**, respectively. **2B** could be recovered upon the addition of acetone to **2G**, **2Y**, and **2O**. Thus, these four emitting solid states of **2** can be switched between repeatedly by means of acetone soaking and the application of mechanical stimulation. Importantly, single crystal and powder X-ray diffraction (PXRD) studies fully show the detailed molecular arrangements of **2B**, **2G**, and **2Y**. This is the first mechanochromic compound to show interconvertible four color emission in the solid state. We also present the first example of using PXRD measurements and the Rietveld refinement technique for the structural analysis of a ground powder in a luminescence mechanochromism study. We obtained complete molecular-level structural information of the crystalline states of **2B**, **2G**, **2Y**, and **2O**. In comparison with a more solvophobic analogue **1**, we suggest that the weak interaction of **2** with acetone in the solid state would allow a solvent inclusion/release mode, which is an important structural factor for the unprecedented multicolor mechanochromic luminescence.

Received 20th December 2014
Accepted 21st January 2015

DOI: 10.1039/c4sc03960b

www.rsc.org/chemicalscience

Introduction

Solid compounds that show a visible response upon mechanical stimulation have recently emerged as interesting smart materials. A mechanical stimulus, typically grinding or shearing, induces a luminescence or color change of the solid compounds, which is referred to as mechanochromism.[1] These materials are promising in sensory and recording applications. Further development of smarter functions, such as multicolor mechanochromism with a detailed understanding of the relationship between structural and optical properties, is desirable. Most luminescent mechanochromic compounds show a single-step phase change upon application of a mechanical force, and there have only been a few reports of materials exhibiting dual emission color changes upon mechanical stimulation. Kato reported a brightly tricolored mechanochromic anthracene derivative which took advantage of the phase change of the liquid crystalline phase.[2] Jia reported a mechanical force strength-dependent mechanochromic molecule containing two different chromophore units, which exhibited two individual emission color changes.[3] The group of Yamaguchi and Saito found that tetrathiazolyl thiophene exhibits distinct emission color changes with a change of pressure and shearing force.[4] More recently, the Yagai and Ito group reported the rational design of a mechanochromic compound with dipolar and amphiphilic character that showed a two-step emission color change by mechanical stimulation.[5] However, solid materials that show multiple luminescence color changes are still rare. To the best of our knowledge, no mechanochromic materials that show tetracolored luminescence changes have been reported.

[a]*Division of Chemical Process Engineering and Frontier Chemistry Center, Faculty of Engineering, Hokkaido University, Sapporo, Hokkaido, 060-8628, Japan. E-mail: hajito@eng.hokudai.ac.jp*

[b]*Catalysis Research Center, Hokkaido University, Sapporo, Hokkaido, 001-0021, Japan*

[c]*Department of Chemistry and Materials Science, Graduate School of Tokyo Institute of Technology, Meguro-ku, Tokyo, 152-8551, Japan*

† Electronic supplementary information (ESI) available: X-ray crystallographic data, optical properties, characterization and interconversion of **2B**, **2G**, **2Y** and **2O**, and other additional information. CCDC 1035806, 1035808 and 1035810. For ESI and crystallographic data in CIF or other electronic format see DOI: 10.1039/c4sc03960b

The luminescence properties of molecules that show luminescent mechanochromism are very sensitive to environmental changes around the molecules and are strongly related to their solid state structures. In a typical case of luminescent mechanochromism, the crystalline structure of the mechanochromic compound is changed to an amorphous phase, which exhibits a different luminescence color from that observed in its crystalline state.[3,6] The amorphous phase can revert to the original crystalline structure through recrystallization by solvent fuming or heating. We previously reported the first demonstration of the reversible luminescent mechanochromism of **1** based on this mechanism (Fig. 1 and 2a).[6a] Mechanical grinding or shearing is non-coherent and exerts random stimulation on the solid. Thus, these mechanical stresses tend to induce a crystalline-to-amorphous phase transition, in which the latter phase has a random structure when compared with the former. Approximately 80% of reported crystalline mechanochromic luminescent materials show this type of phase transition.[3,6] Some mechanochromic compounds cocrystallize with a solvent and yield an amorphous phase after grinding, accompanied by solvent release.[7] Luminescent mechanochromism caused by the conversion of one crystal structure to another with a different molecular arrangement constitutes only 10% of mechanochromic luminescent materials.[4,8] More remarkable mechanisms, such as mechano-triggered single-crystal-to-single-crystal phase transition of mechanochromic gold(I) isocyanide complexes, have been reported by our group.[9] In most examples, luminescent mechanochromism compounds can only show a single phase transition upon mechanical stimulation. Multiple phase transitions can realize multiple responses; however, such materials have been rarely reported.

One obstacle facing researchers in the study of mechanochromism is the difficulty of the structural analysis of the powdery solid samples obtained after the mechanical process. This is in contrast to solid structure analyses before mechanical stimulation of the sample, in which the crystalline material can be analyzed by single crystal X-ray analysis. Powder X-ray diffraction (PXRD) measurements and Rietveld refinement techniques are known to be powerful methods for crystalline structure analyses of powdered materials;[10] however, there have been no reports of this method being applied to mechanochromic materials.

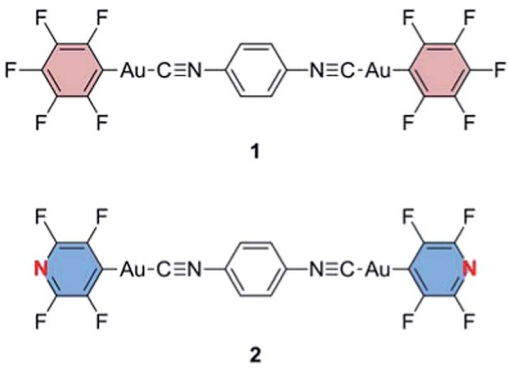

Fig. 1 Structures of gold(I) isocyanide complexes **1** and **2**.

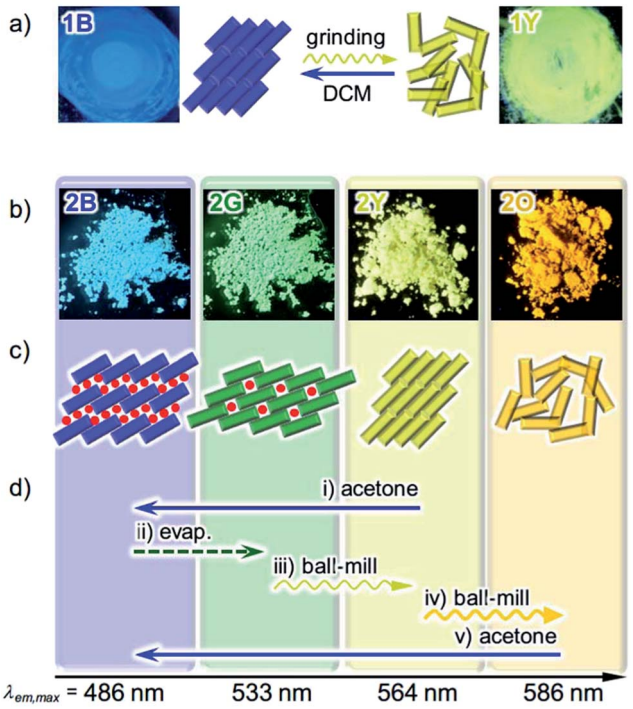

Fig. 2 (a) Photographs and schematic representation of the molecular arrangements of **1** showing different photoluminescence upon applying external stimuli. A molecule of **1** is denoted as a rectangle. (b) Photographs of the powder forms of **2** showing different photoluminescence under UV light at 365 nm. (c) Schematic representation of the solid state molecular arrangements of **2**, in which a molecule of **2** is denoted as a rectangle, with the colors of the corresponding emission. Solvent molecules are denoted as red circles. (d) Specific procedures for the interconversion of the four emitting states of **2**.

In this paper, we report a new mechanochromic luminescent material **2** (Fig. 1), showing crystal-to-crystal-to-amorphous phase changes upon mechanical grinding and solvent-related structural modifications. As a result, compound **2** shows four individual solid state emissions, which are interconvertible by the addition of solvent and application of mechanical force (Fig. 2b–d). We studied the optical properties and single crystal and powder X-ray diffraction analyses of the new compound **2**. For the first time, we solved the crystalline structures of ground powders of the luminescent mechanochromic compound by PXRD measurements and Rietveld refinement. Thermal analyses of **2** provide the unique profile features of its crystalline structure change upon mechanical stimulation. Compound **2** is shown to be the first mechanochromic compound incorporating four interconvertible structures with different emission properties. The structural analysis reveals that weak interactions between the solvent and **2** created the solvent releasing crystal-to-crystal conversion, which is an unprecedented mechanochromic structural change. The combination of two crystal-to-crystal phase changes and one crystal-to-amorphous phase change results in the novel interconversion between four different colors.

Results and discussion

Stimuli-responsive emission color changes

We previously reported the reversible two-colored luminescent mechanochromism of gold(I) isocyanide complex **1**, exhibiting a phase transition from blue-emitting **1B** to yellow-emitting **1Y** (Fig. 2a).[6a] This emission color change arises from the crystalline-to-amorphous phase transition as revealed by the PXRD pattern. We suggested that the yellow emission in amorphous ground powder **1Y** was responsible for the formation of aurophilic interactions.[1d,e,11,12] The original blue emission was recovered upon the addition of dichloromethane to **1Y**, owing to partial dissolution followed by recrystallization. The role of dichloromethane is to facilitate the recrystallization of amorphous **1Y** to crystalline **1B**. Both **1B** and **1Y** are solvophobic and do not contain any solvent in their crystal lattice.

The new complex **2** shows four individual emission colors which are interconvertible by treatment with acetone and mechanical stimulation (Fig. 2b–d). The as-synthesized yellow solid of **2** exhibits yellow emission under UV light irradiation at 365 nm and thus is referred to as **2Y** (Fig. 2b). The emission color of **2Y** immediately turns into blue upon soaking the powder in acetone (step (i) in Fig. 2d and S1†), and the resulting polymorph is referred to as **2B**. It should be noted that complex **2** is scarcely soluble in acetone (c_{max} = 0.2 mg mL^{-1}) and its acetone solution is not emissive in the visible region.[13] Upon air drying, the polymorph **2B** immediately transforms to a green-emitting polymorph **2G** (step (ii) in Fig. 2d and S1†). **2G** may contain acetone molecules in the crystal lattice, but did not show any further emission color changes even under reduced pressure for weeks. When **2G** was ground using a pestle, yellow and orange emissions were observed upon gentle and hard grinding, respectively (Fig. S2a†). After several experiments, we determined that two different solid states with distinct emissions emerge in a stepwise fashion by ball-milling over a short and long duration (Fig. S2b†). When **2G** was mechanically stimulated in a ball-mill at 4600 rpm for 10 min (short grinding), the emission color of the powder was yellow (step (iii) in Fig. 2d), indicating the recovery of **2Y**. When **2Y** is ground by ball-milling for an additional 5 min (long grinding), orange colored emission was observed, corresponding to the formation of **2O** (step (iv) in Fig. 2d). Similar mechano-responsive stepwise emission color changes have rarely been reported in the literature.[3,5] After further grinding of **2O** for 1 h, no subsequent changes in the orange emission are observed. The reversion of **2O** to **2B** occurs by soaking the powder in acetone (step (v) in Fig. 2d), indicating the interconvertibility between the four emission colors of **2**.[14] The following solid state spectroscopic studies of **2** indicate that treatment with acetone induces crystalline structure changes with blue-shifted emission (steps (i) and (v) in Fig. 2d), whereas mechanical grinding results in those with red-shifted emission (steps (iii) and (iv) in Fig. 2d).

The optical properties of the four emitting solid states of **2** were investigated by steady-state spectroscopy (Fig. 3). Under excitation at 365 nm, all of the solid materials of **2** show broad emission bands that are devoid of vibrational structures (solid lines in Fig. 3). The emission spectra of **2B**, **2G**, **2Y**, and **2O** have maxima at 486, 533, 564, and 586 nm, respectively, confirming the wide coverage of the visible spectral region. This is in contrast to the THF solution of **2** which is not emissive [absolute emission quantum yield (Φ_{em}) is 0%, Fig. S3†]. This indicates that the solid state emission properties of **2** are dependent on aggregation in the solid phase. The excitation spectra of **2B**, **2G**, **2Y**, and **2O** detected at the emission maxima show broad bands with peaks at 385, 415, 397, and 459 nm, respectively (dashed lines, Fig. 3). The UV-vis absorption spectrum of the THF solution of **2** showed an absorption band in the range of 200–300 nm (Fig. S4†), shorter than the regions of the excitation bands observed for **2B**, **2G**, **2Y**, and **2O**. The different excitation spectra suggest that the ground state structures of **2B**, **2G**, **2Y**, and **2O** in the solid phase are distinct from each other.

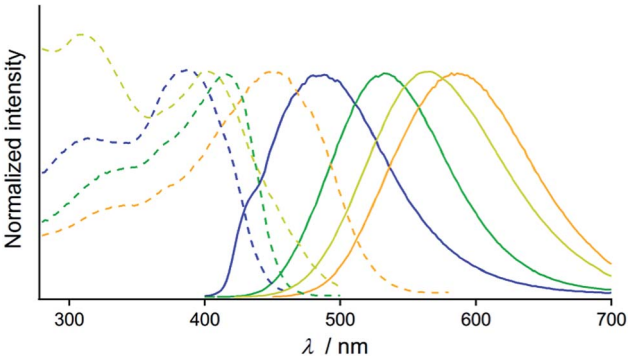

Fig. 3 Normalized excitation (dashed lines, monitored at the emission maxima) and emission spectra (solid lines, λ_{em} = 365 nm) of 2B (blue lines), 2G (green lines), 2Y (yellow lines), and 2O (orange lines).

Photophysical properties were investigated for the powders of **2** with different emission properties and the results are summarized in Table S1.† The Φ_{em} of **2B** and **2G** are both 10%, whereas Φ_{em} of **2Y** and **2O**, both obtained by ball-milling, are 27 and 30%, respectively (Table S1†). Mechanical force-induced emission color change with increased Φ_{em} was reported for organometallic complexes.[6a,9b] Photoluminescence lifetime spectroscopy was also carried out and the emission decay profiles are presented in Fig. S5†. The emission decay profiles of **2B**, **2G**, **2Y**, and **2O** were all fitted to a biexponential curve. The average lifetime τ_{av} [$=(\sum A_i\tau_i)/(\sum A_i)$] of **2G**, **2Y**, and **2O** are almost the same, within the range of 0.4–0.7 μs (Table S1†). However, a longer τ_{av} value of 2.55 μs was observed for **2B**.

Stimuli-responsive crystalline structure changes

PXRD measurements indicate that **2B**, **2G**, **2Y**, and **2O** have distinct packing arrangements. It has been reported that the emission properties of solid materials are significantly related to their crystalline structures and the intermolecular interaction patterns.[15] The powders of **2B**, **2G**, and **2Y** showed several intense diffractions (Fig. 4), indicating their crystalline nature. The diffraction of **2Y**, obtained by short grinding (ball-milling for 10 min), is principally similar to that of the as-synthesized powder (Fig. S6†), consistent with the similarity in their emission. Moreover, the PXRD patterns indicate that crystalline-to-

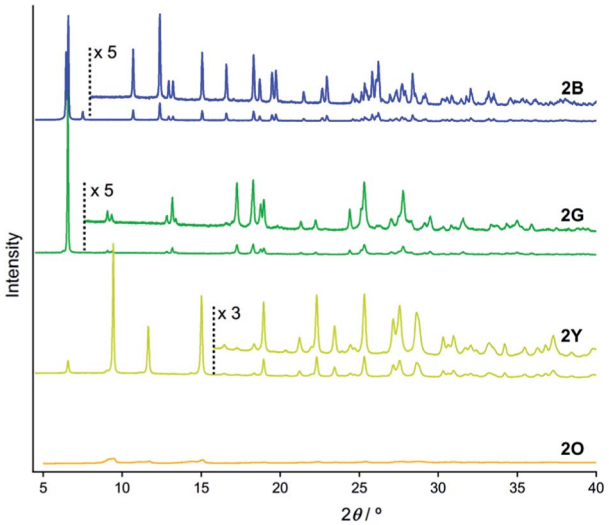

Fig. 4 PXRD patterns of **2B** (blue line), **2G** (green line), **2Y** (yellow line), and **2O** (orange line).

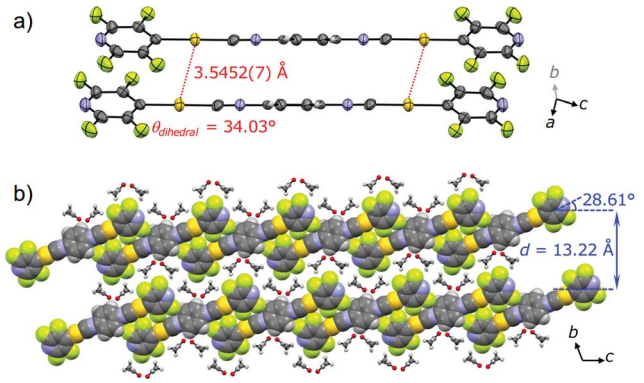

Fig. 5 (a) ORTEP representation of the dimer and (b) the space-filling representation of the packing structure of **2B** viewed along the direction of the *a* axis. Acetone molecules are depicted as ball-and-stick models in (b).

crystalline phase transition from **2G** to **2Y** occurs upon mechanical stimulation.[4,8] Unlike the above three patterns, the PXRD pattern of **2O** showed diffractions with very small intensity (orange line in Fig. 4), indicating that **2O** is in an amorphous phase. The crystalline-to-amorphous phase transition from **2Y** to **2O** is likely a result of the long grinding (ball-milling for 15 min) disrupting the ordered molecular arrangements as is commonly observed for mechanochromic compounds.[3,6] The four different diffraction patterns of **2B**, **2G**, **2Y**, and **2O** indicate that each of their crystalline arrangements are distinct. As multicolored luminescent mechanochromic compounds have rarely been reported,[2–5] the relationship between their detailed crystalline structures and emission properties should give useful insight.

To gain a better understanding of the structure–property relationship of **2B**, we performed single crystal X-ray diffraction analysis. The blue-emitting single crystal was prepared from a saturated acetone solution of **2**. **2B** crystallized in the triclinic system $P\bar{1}$ (Fig. 5, Table 1 and S2†). The central isocyanide benzene ring of the molecule is on the inversion center. The simulated powder pattern obtained from the single crystal structure is identical to the PXRD pattern of **2B** (Fig. S7a†). Molecules in **2B** form a layer-like structure with an interlayer spacing, *d*, of 13.22 Å in which the molecular tilt angle is 28.61°. For each molecule, the dihedral angle $\theta_{\mathrm{dihedral}}$ between the central benzenes and lateral pyridines is 34.03°. Within the layer, the molecules form four CH···F intermolecular interactions with the adjacent two molecules (Fig. S8†) to construct a tape-like motif. **2B** contains 2 equivalents of disordered acetone molecules which form sublayers between the tape-like structures of **2** (**2B**: [**2**] × 2 = [acetone]; Fig. 5b). The gold molecules in the tapes and the acetone molecules in the sublayers interact *via* CH···O and CH···F intermolecular interactions (Fig. S8†). The absence of defined intermolecular interactions between the tapes, owing to the presence of the acetone sublayers, is thought to make **2B** unstable under acetone-free conditions. The molecules in the tapes stack on top of each other without a prominent longitudinal offset through π–π stacking interactions between both the benzene rings and between the pyridine rings with perpendicular distances of 3.314 and 3.334 Å, respectively. These intermolecular interactions in the tapes of **2B** may play an important role in achieving a longer wavelength emission compared with that of the solution phase. However, the Au···Au distance of 3.5452(7) Å (Fig. 5a) is beyond the limit of aurophilic interactions, which indicates their negligible influence on the emission energy level of **2B**.

The single crystal X-ray diffraction analysis of **2G** provides information on the origin of the emission color change. For preparation of the single crystal **2G**, single crystal **2B** was exposed either to air or water vapor to remove the incorporated acetone molecules. The resulting green-emitting crystals obtained by both methods afforded similar packing structures

Table 1 Summary of the crystal structure analyses of **2B**, **2G**, and **2Y**

	2B	**2G**	**2Y**
CCDC number	1035806	1035808	1035810
Specimen	Single crystal	Single crystal	Powder
Crystal system	Triclinic	Triclinic	Monoclinic
Space group	$P\bar{1}$ (#2)	$P\bar{1}$ (#2)	$P2_1/c$ (#14)
a/Å	3.5452(4)	3.5707(3)	7.79058(18)
b/Å	14.0087(15)	10.3087(10)	18.7202(5)
c/Å	14.2490(15)	14.2742(11)	6.74157(17)
α/°	109.292(3)	107.689(4)	90
β/°	91.673(3)	92.505(5)	103.167(3)
γ/°	91.322(2)	100.205(5)	90
V/Å^3	667.23(13)	489.99(8)	957.35(5)
Z value	1	1	2
D_{calc}/g cm^{-3}	2.335	2.786	—
$R_1{}^a$/%	4.73	10.08	—
w$R_2{}^b$/%	10.55	25.46	—
GOF^c	1.152	1.114	—
R_{wp}/%	—	—	4.62
R_{p}/%	—	—	3.60
R_{F2}/%	—	—	2.74

[a] For data with $I > 2.00\sigma(I)$. [b] For all reflection data. [c] Goodness of fit.

and the latter method yielded better diffraction data. Both methods are observed to yield **2G** because their simulated powder patterns are identical to the PXRD pattern of **2G** (Fig. S7b†). **2G** crystallized in the triclinic space group $P\bar{1}$ (Fig. 6, Table 1 and S2†). The central isocyanide benzene ring of the molecule is on the inversion center. **2G** forms layered structures (Fig. 6b) similar to **2B**. The layer spacing, *d*, of **2G** is 9.821 Å in which the molecular tilt angle is 21.66°. In **2G**, a 1-D channel structure with some residual electron density along the *a* axis exists between the molecular tape structures (Fig. S9a†), indicating the inclusion of a small amount of acetone molecules. Based on the X-ray diffraction analyses and ^{1}H NMR spectroscopy, the included acetone molecules in **2G** are less than 0.5 equivalents (**2G**: [**2**] × *n* = [acetone], *n* < 0.5).[16] Owing to the lack of an "acetone sublayer" in **2G**, the gold complexes in the tape structure of **2G** can interact with adjacent complexes through multipoint F···F and CH···F interactions (Fig. S9b†). As a result, flat 2-D sheets which extend along the *bc*-planes are formed. Between sheets, molecules stack on top of each other without offset through π–π stacking interactions with a perpendicular distance of 3.509 Å (benzene rings) and 3.330 Å (pyridine rings). **2G** does not contain aurophilic interactions [Au···Au separation: 3.571(2) Å] (Fig. 6a). The smaller excitation energy of **2G** compared with that of **2B** may be caused either by smaller amounts of solvent inclusion, which may enhance chromophore–chromophore interactions, or by the rather flat conformations of the chromophore ($\theta_{dihedral} = 11.92°$), which may lead to an effective intra and/or intermolecular conjugation.[17]

PXRD measurements and Rietveld refinement disclosed the detailed crystalline structure of **2Y** demonstrating that its yellow emission is caused by aurophilic interactions. The molecular packing arrangement of **2Y** was determined with suitable quality from the PXRD data with a range of 2θ = 7–60° (Fig. S10†).[18] It should be noted that the present study is the first example showing the great advantage of *ab initio* structural analysis of ground powders of mechanochromic compounds.[19] Ground powder **2Y** crystallizes in the monoclinic space group $P2_1/c$ (Fig. 7 and Table 1 and S3†). The central isocyanide benzene ring of the molecule is on the inversion center. The molecular packing arrangement of **2Y** is rather different from those of **2B** and **2G**. For example, no solvent molecules exist in

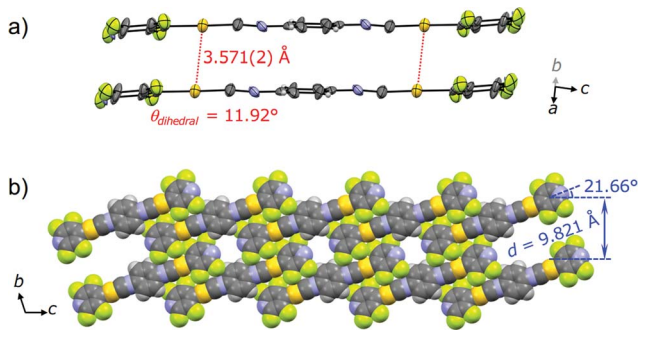

Fig. 6 (a) ORTEP representation of the dimer viewed roughly along the direction of the *b* axis and (b) space-filling representation of the packing structure of **2G** viewed along the direction of the *a* axis.

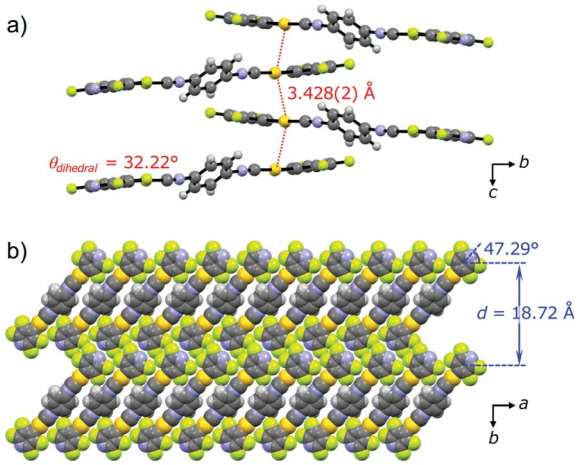

Fig. 7 (a) Ball-and-stick representation of the tetramer viewed along the direction of the *a* axis, and (b) the space-filling representation of the packing structures of **2Y** viewed along the direction of the *c* axis.

the crystalline lattice of **2Y**, which is also supported by thermal analysis, elemental analysis and ^{1}H NMR spectroscopy (Fig. 8 and S13 and Table S4†). Moreover, face-to-face stacking of the molecules is absent. Instead, infinite chains of Au···Au interactions with a distance of 3.428(2) Å are formed along the direction of the *c* axis (Fig. 7a). This distance is within the range of aurophilic interactions, and is likely to be responsible for the emission properties of **2Y** with a low excited energy level. Perpendicular to the aurophilic bond, molecules afford a flat sheet through multipoint F···F interactions between the tape-like motif (Fig. S11a†). Within the sheet, all the molecular long axes are oriented along the same direction, and in the adjacent sheet molecules are oriented at approximately 90° with respect to those in the next layer (Fig. S11b†). This is the first report of mechano-induced crystal-to-crystal phase conversion with solvent release.

The orange emission of **2O**, with the smallest excitation energy of the four different structures of **2**, is attributed to the aurophilic bonds with the shortest Au···Au distance. Owing to the amorphous nature, the detailed intermolecular interaction patterns existing in **2O** are unclear. TGA, elemental analysis and the ^{1}H NMR spectrum revealed that **2O** contains no solvent molecules (Fig. 8 and S14 and Table S4†), therefore chromophore–chromophore interactions, rather than chromophore–solvent interactions, must be involved. From the longest wavelength maxima in the excitation and emission spectra, it is more likely that aurophilic interactions with shorter Au···Au separation compared with those observed in **2Y** should be present.[6a] In the amorphous ground phase of mechanochromic organometallic compounds, it is reported that metallophilic bonds are formed that effect their emission properties.[6a,b,7e,g]

The above discussion indicates that **2** can form two solvated (**2B** and **2G**) and two non-solvated (**2Y** and **2O**) solid states. This can be confirmed by the experimental results of the crystal structure analyses, thermal analyses, elemental analyses and ^{1}H NMR spectroscopy as mentioned above (see the ESI†). This is further supported by IR spectroscopy: the IR spectra of **2B** and

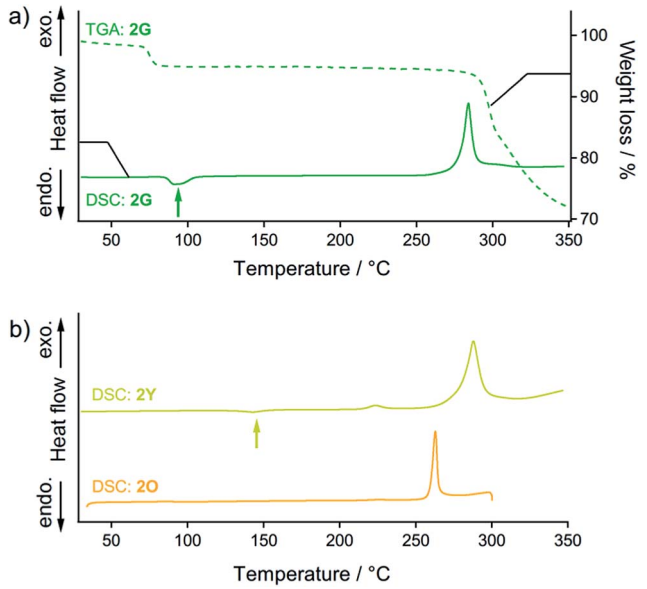

Fig. 8 (a) DSC (solid line) and TGA (dashed line) profiles of **2G**. The green arrow indicates the endothermic phase transition from **2G** to **2Y**. (b) DSC profiles of **2Y** (yellow line) and **2O** (orange line). The yellow arrow indicates the endothermic phase transition from **2Y** to **2O**. For the DSC and TGA profiles, the heating rate is 10 °C min^{-1}.

2G show carbonyl stretching vibrational bands at around 1715 cm^{-1}, while those of **2Y** and **2O** do not (Fig. S15†). Therefore, crystalline structure changes with solvent inclusion/release mode are important for the interconvertible multiple photoluminescence color of **2**.

Thermal analyses

Thermal analysis of **2G** (Fig. 8a) reveals that its phase transition into the **2Y** phase occurs with solvent release. DSC measurements of **2G** show the endothermic peak at 95 °C (green arrow in Fig. 8a) before observation of the prominent exothermic peaks of decomposition above 250 °C. The endothermic peak at 95 °C can be attributed to the thermal phase transition from **2G** to **2Y**[20] because the emission color of **2G** changed from green to yellow at this temperature (Fig. S16†). This phase transition (**2G** → **2Y**) occurs with solvent release: the TGA profile of **2G** reveals a 5% weight loss at around at 90 °C (dashed line in Fig. 8a). This result suggests that the phase transition of **2G** by short grinding also induces solvent release to form **2Y**.[21] Although mechanochromism with solvent release was reported previously,[7] this is the first report of a crystal-to-crystal phase conversion.

DSC analyses show the relative thermodynamic stability of the solvent-free forms of **2Y** and **2O**.[22] DSC measurements of **2Y** show the endothermic peak of the phase transitions at around 145 °C (yellow arrow in Fig. 8b). The emission color change of **2Y** from yellow to orange was also observed at around 160 °C upon heating treatment (Fig. S16†). Thus, the endothermic peak of **2Y** at 145 °C can be attributed to the thermal phase transition from **2Y** to **2O**. The TGA profile of **2Y** does not show any discernible weight loss in this temperature range, because no solvent is included (Fig. S17†). However, DSC and TGA profiles of **2O** do not show any peaks until decomposition above 250 °C (orange line in Fig. 8b and S17†), owing to the absence of the phase transition upon heating. This is supported by the fact that the thermal-induced emission color change of **2O** is absent (Fig. S16†). From these results, **2Y** can be considered as the solvent-free metastable polymorph of **2**, while **2O** is the solvent-free, thermodynamically more stable phase.[23]

The fact that the phase transition from **2G** to **2Y** requires solvent release and that **2Y** is less thermodynamically stable than **2O** is key to realize a unique two-step mechanochromism, **2G** → **2Y** → **2O** (steps (iii) and (iv) in Fig. 2d). In the initial stage of grinding of **2G** (step (iii) in Fig. 2d), included solvent molecules start to be released owing to decreasing the particle size and increasing the surface area of the solid sample. This initiates molecular rearrangement of **2G** to give the solvent-free form. As a result, **2Y** is initially formed as a kinetically trapped metastable intermediate. Additional mechanical stimulation provides the **2O** phase (step (iv) in Fig. 2d), which is the more thermodynamically stable form of **2**. This type of crystal-to-amorphous phase transition (**2Y** → **2O**) upon mechanical stimulation in a solvent-free solid state condition is most commonly observed for mechanochromic compounds.[3,6] As mentioned above, we confirm that **2B** and **2G** contain solvent molecules in their crystalline lattices while **2Y** and **2O** do not contain any solvent molecules based on crystal structure analyses, thermal analyses, elemental analyses and ^{1}H NMR and IR spectroscopy (see the ESI†).

Role of tetrafluoropyridyl groups on the unique stimuli-responsivity of 2

It is surprising that substitution of the pentafluorophenyl group in **1** by a tetrafluoropyridyl group in **2** leads to a dramatic enhancement of its stimuli-responsivity (Fig. 2). It has been reported that subtle modifications of chemical structure can induce a significant change in solid state structures.[15] As the overall crystalline structures are generally determined by accumulation of relatively weak intermolecular interactions, it is sometimes difficult to understand the relationships between molecular and crystalline structures. Indeed, at this stage, it is difficult to fully determine which molecular structural factor of **2** is important for its unique stimuli-responsivity.

However, one possible explanation for the impact of the molecular structure on the mechanochromic properties concerns the relatively high polarity of **2** (Fig. S18†), which may help the formation of weak interactions with acetone. For the previously reported solvophobic complex **1** containing a C_6F_5 moiety, the molecules in the crystals were densely packed, and no solvent inclusion was observed.[6a] Complex **2**, with a C_5NF_4 moiety, is more polar and less solvophobic compared to **1**. This enables the solvent inclusion/release process owing to the weak interactions between the polar molecule **2** and acetone. In the presence of many solvent molecules, blue-emitting **2B** was formed, then after evaporation of acetone, the less solvated **2G** was formed. As the solvated acetone molecules were weakly absorbed in the crystal lattice, weak mechanical stimulation induces solvent release to produce non-solvated **2Y**. The slight

molecular structural change from **1** with the C_6F_5 moiety to less solvophobic **2** with the C_5NF_4 moiety is an important key factor to realize unprecedented crystal-to-crystal-to-amorphous phase transition with the different emission color changes.

Conclusions

We report complex **2** which can adopt four different solid state structures with different emission properties. The four different emissions of **2** in the solid state are reversible. Multiple switching of the solid state emission of **2** was caused by a combination of dual two-step emission color changes which are induced by solvent inclusion/release and short/long mechanical stimulation. In an acetone atmosphere, blue-emitting **2B** was formed, and after acetone release, green-emitting **2G** was formed. Upon applying a mechanical stimulus to **2G**, two-step emission color changes to yellow (short ball-milling) and then to orange (long ball-milling) were observed, which correspond to phase changes into **2Y** and **2O**, respectively. Single crystal and powder X-ray diffraction analyses successfully revealed the detailed molecular arrangements of **2B**, **2G**, and **2Y**. We found that both **2B** and **2G** formed solvated crystalline structures without defined aurophilic interactions. Conversely, the **2Y** powder formed a solvent-free ordered molecular arrangement involving aurophilic interactions. The amorphous **2O** phase is suggested to contain aurophilic interactions with the shortest Au···Au distance. Thermal analyses revealed that the phase transition from **2G** to **2Y** requires solvent release. Moreover, the amorphous **2O** phase is thermodynamically more stable than the **2Y** phase. Thus, this unique two-step mechanochromism (**2G** → **2Y** → **2O**) upon mechanical stimulation starts with solvent release from **2G** followed by rearrangement into solvent-free **2Y** (crystal-to-crystal phase transition), and then crystal-to-amorphous phase transition takes place to form the thermodynamically more stable **2O**. Comparison between **1** with a C_6F_5 moiety and **2** with a C_5NF_4 moiety suggests that the more polar and less solvophobic nature of **2** may create the solvent inclusion/release structure transition. This is an important factor for the multiple structures and emission color transformation of **2**. The present multicolored mechanochromic complex **2** with fully-solved structures can be considered as a new type of smart material.

Experimental section

Synthesis of 2,3,5,6-tetrafluoropyridyl(tetrahydrothiophene) gold(I)

2,3,5,6-Tetrafluoropyridine (755.3 mg, 5.0 mmol) was dissolved in dry THF (20 mL) with stirring at −78 °C in a 100 mL round-bottomed flask, then *n*-BuLi (1.65 M hexane) was added dropwise for 15 min. After 1 h, chloro(tetrahydrothiophene)gold(I) (1.92 g, 6.0 mmol) was added to the reaction mixture. Then, the mixture was allowed to warm to room temperature and was stirred for 1 h. Addition of a small portion of water quenches the reaction. $MgSO_4$ was added to the mixture and stirred for 20 min. $MgSO_4$ was filtered off by filtration and the solvent was evaporated. The residue was quickly passed through a short silica gel column (CH_2Cl_2–hexane = 50 : 50, 100 mL) to give a white-purple solid (1.72 g, 4.0 mmol, 79%). ^{1}H NMR [400 MHz, $CDCl_3$, δ (ppm)]: 2.24 (s, 4H), 3.46 (s, 4H). ^{13}C NMR [100 MHz, $CDCl_3$, δ (ppm)]: 30.7 (*C*H$_2$), 38.7 (*C*H$_2$), (*C*H), 141.7 (*C*H), 143.9 (*C*H), 144.3 (*C*H). HRMS-FAB (*m*/*z*): [M + H] calcd for $C_{19}H_9AuNF_4^+$, 436.0052; found, 436.0058. Anal. calcd for $C_{19}H_8AuNF_4$: C, 24.84, H, 1.85; N, 3.22. Found: C, 24.87; H, 1.90; N, 3.05.

Synthesis of 2

A mixture of 1,4-diisocyanobenzene (64.1 mg, 0.5 mmol) and 2,3,5,6-tetrafluoropyridyl(tetrahydrothiophene)gold(I) (435.2 mg, 1.0 mmol) in CH_2Cl_2 (5 mL) was stirred for 30 min under a N_2 atmosphere at room temperature. The precipitates were filtered and washed with CH_2Cl_2, and dried *in vacuo* to obtain **2** as a yellow solid (350.3 mg, 0.4 mmol, 85%). ^{1}H NMR (400 MHz, THF-d_8, δ (ppm)): 8.14 (s, 4H). The poor solubility of **2** in solvents hampered ^{13}C NMR measurements. HRMS-FAB (*m*/*z*): [M + H] calcd for $C_{18}H_5Au_2N_4F_8^+$, 822.9712; found, 822.9711. Anal. calcd for $C_{18}H_4Au_2N_4F_8$: C, 26.30, H, 0.49; N, 6.81. Found: C, 26.23; H, 0.64; N, 6.63.

Preparation of 2B

The blue luminescent powder **2B** was prepared from **2Y**, **2G**, and **2O** immediately after they were soaked in acetone. IR (neat): $\tilde{\nu}$ = 2218, 1704, 1628, 1543, 1421, 1214, 927, 832 cm^{-1}.

Preparation of 2G

Upon air drying a powder of **2B** to evaporate acetone, green-emitting **2G** was immediately formed. IR (neat): $\tilde{\nu}$ = 2209, 1628, 1453, 1207, 929, 838 cm^{-1}. ^{1}H NMR [400 MHz, THF-d_8, Fig. S12,† δ (ppm)]: 8.14 (s, 4H). The methyl proton of included acetone was also observed at 2.11 ppm. Anal. calcd for $C_{18}H_4Au_2N_4F_8$: C, 26.30, H, 0.49; N, 6.81. Found: C, 26.67; H, 0.89; N, 6.63.

Preparation of 2Y

As-prepared solid **2Y** was analytically pure but, in terms of the crystalline arrangement, it is impure as shown by the PXRD pattern (Fig. S6†). For purification of as-synthesized **2Y**, **2** was suspended in cyclohexanone (c_{max} = 1 mg mL^{-1}) and filtered and washed with that solvent, then dried *in vacuo* to give the yellow-emitting powder **2Y**. An alternative preparation method for **2Y** is to grind **2G** in a ball-mill at 4600 rpm for 10 min (Taitec Bead Crusher μT-01). Typically, **2G** (50 mg) and a stainless bead (1/8 inch) were put into a micro tube (ϕ13 × 49 mm) with a screw cap and ball-milled for 10 min, during which time the container should be opened two or three times to facilitate solvent release. IR (neat): 2217, 1620, 1420, 1207, 921, 838 cm^{-1}. ^{1}H NMR [400 MHz, THF-d_8, Fig. S13,† δ (ppm)]: 8.14 (s, 4H). Anal. calcd for $C_{18}H_4Au_2N_4F_8$: C, 26.30, H, 0.49; N, 6.81. Found: C, 26.39; H, 0.60; N, 6.79.

Preparation of 2O

For the preparation of **2O**, **2Y** was ground in a ball-mill at 4600 rpm for 5 min. IR (neat): $\tilde{\nu}$ = 2204, 1620, 1421, 1201, 916, 829 cm^{-1}. ^1H NMR [400 MHz, THF-d_8, Fig. S14,† δ (ppm)]: 8.14 (s, 4H). Anal. calcd for $C_{18}H_4Au_2N_4F_8$: C, 26.30, H, 0.49; N, 6.81. Found: C, 26.23; H, 0.64; N, 6.63.

Acknowledgements

This work was financially supported by the Funding Program for Next Generation World-Leading Researchers (NEXT Program, no. G002) from the Japan Society for the Promotion of Science (JSPS), the MEXT (Japan) program "Strategic Molecular and Materials Chemistry through Innovative Coupling Reactions" of Hokkaido University, and JSPS KAKENHI Grant-in-Aid for Challenging Exploratory Research, 26620053, and for Young Scientists (B), 26810042. We also thank the support of Frontier Chemistry Center Akira Suzuki "Laboratories for Future Creation" Project.

Notes and references

1 (*a*) Z. Chi, X. Zhang, B. Xu, X. Zhou, C. Ma, Y. Zhang, S. Liu and J. Xu, *Chem. Soc. Rev.*, 2012, **41**, 3878–3896; (*b*) X. Zhang, Z. Chi, Y. Zhang, S. Liu and J. Xu, *J. Mater. Chem. C*, 2013, **1**, 3376–3390; (*c*) Y. Sagara and T. Kato, *Nat. Chem.*, 2009, **1**, 605–610; (*d*) A. L. Balch, *Angew. Chem., Int. Ed.*, 2009, **48**, 2641–2644; (*e*) C. Jobbágy and A. Deák, *Eur. J. Inorg. Chem.*, 2014, **2014**, 4434–4449.

2 Y. Sagara and T. Kato, *Angew. Chem., Int. Ed.*, 2011, **50**, 9128–9132.

3 Z. Ma, M. Teng, Z. Wang, S. Yang and X. Jia, *Angew. Chem., Int. Ed.*, 2013, **52**, 12268–12272.

4 K. Nagura, S. Saito, H. Yusa, H. Yamawaki, H. Fujihisa, H. Sato, Y. Shimoikeda and S. Yamaguchi, *J. Am. Chem. Soc.*, 2013, **135**, 10322–10325.

5 S. Yagai, S. Okamura, Y. Nakano, M. Yamauchi, K. Kishikawa, T. Karatsu, A. Kitamura, A. Ueno, D. Kuzuhara, H. Yamada, T. Seki and H. Ito, *Nat. Commun.*, 2014, **5**, 4013.

6 (*a*) H. Ito, T. Saito, N. Oshima, N. Kitamura, S. Ishizaka, Y. Hinatsu, M. Wakeshima, M. Kato, K. Tsuge and M. Sawamura, *J. Am. Chem. Soc.*, 2008, **130**, 10044–10045; (*b*) K. Kawaguchi, T. Seki, T. Karatsu, A. Kitamura, H. Ito and S. Yagai, *Chem. Commun.*, 2013, **49**, 11391–11393; (*c*) N. D. Nguyen, G. Zhang, J. Lu, A. E. Sherman and C. L. Fraser, *J. Mater. Chem.*, 2011, **21**, 8409–8415; (*d*) S. H. Lim, M. M. Olmstead and A. L. Balch, *Chem. Sci.*, 2013, **4**, 311–318; (*e*) H. Sun, S. Liu, W. Lin, K. Y. Zhang, W. Lv, X. Huang, F. Huo, H. Yang, G. Jenkins, Q. Zhao and W. Huang, *Nat. Commun.*, 2014, **5**, 3601; (*f*) W. Li, L. Wang, J.-P. Zhang and H. Wang, *J. Mater. Chem. C*, 2014, **2**, 1887–1892; (*g*) M. S. Kwon, J. Gierschner, J. Seo and S. Y. Park, *J. Mater. Chem. C*, 2014, **2**, 2552–2557.

7 (*a*) B.-C. Tzeng, T.-Y. Chang and H.-S. Sheu, *Chem.–Eur. J.*, 2010, **16**, 9990–9993; (*b*) J. Ni, X. Zhang, N. Qiu, Y. H. Wu, L. Y. Zhang, J. Zhang and Z. N. Chen, *Inorg. Chem.*, 2011, **50**, 9090–9096; (*c*) S. J. Choi, J. Kuwabara, Y. Nishimura, T. Arai and T. Kanbara, *Chem. Lett.*, 2012, **41**, 65–67; (*d*) N. Zhao, Z. Yang, J. W. Lam, H. H. Sung, N. Xie, S. Chen, H. Su, M. Gao, I. D. Williams, K. S. Wong and B. Z. Tang, *Chem. Commun.*, 2012, **48**, 8637–8639; (*e*) A. Han, P. Du, Z. Sun, H. Wu, H. Jia, R. Zhang, Z. Liang, R. Cao and R. Eisenberg, *Inorg. Chem.*, 2014, **53**, 3338–3344; (*f*) C. Jobbágy, M. Molnár, P. Baranyai, A. Hamza, G. Pálinkás and A. Deák, *CrystEngComm*, 2014, **16**, 3192–3202; (*g*) J. Ni, Y.-G. Wang, H.-H. Wang, Y.-Z. Pan, L. Xu, Y.-Q. Zhao, X.-Y. Liu and J.-J. Zhang, *Eur. J. Inorg. Chem.*, 2014, **2014**, 986–993; (*h*) J. Ni, Y.-G. Wang, H.-H. Wang, L. Xu, Y.-Q. Zhao, Y.-Z. Pan and J.-J. Zhang, *Dalton Trans.*, 2014, **43**, 352–360; (*i*) X.-C. Shan, F.-L. Jiang, L. Chen, M.-Y. Wu, J. Pan, X.-Y. Wan and M.-C. Hong, *J. Mater. Chem. C*, 2013, **1**, 4339–4349; (*j*) X. Zhou, H. Li, Z. Chi, X. Zhang, J. Zhang, B. Xu, Y. Zhang, S. Liu and J. Xu, *New J. Chem.*, 2012, **36**, 685–693.

8 (*a*) N. Harada, Y. Abe, S. Karasawa and N. Koga, *Org. Lett.*, 2012, **14**, 6282–6285; (*b*) N. Harada, S. Karasawa, T. Matsumoto and N. Koga, *Cryst. Growth Des.*, 2013, **13**, 4705–4713; (*c*) S.-J. Yoon, J. W. Chung, J. Gierschner, K. S. Kim, M.-G. Choi, D. Kim and S. Y. Park, *J. Am. Chem. Soc.*, 2010, **132**, 13675–13683; (*d*) M.-S. Yuan, D.-E. Wang, P. Xue, W. Wang, J.-C. Wang, Q. Tu, Z. Liu, Y. Liu, Y. Zhang and J. Wang, *Chem. Mater.*, 2014, **26**, 2467–2477; (*e*) J. Kunzelman, M. Kinami, B. R. Crenshaw, J. D. Protasiewicz and C. Weder, *Adv. Mater.*, 2008, **20**, 119–122.

9 (*a*) T. Seki, K. Sakurada and H. Ito, *Angew. Chem., Int. Ed.*, 2013, **52**, 12828–12832; (*b*) H. Ito, M. Muromoto, S. Kurenuma, S. Ishizaka, N. Kitamura, H. Sato and T. Seki, *Nat. Commun.*, 2013, **4**, 2009.

10 (*a*) K. Fujii, Y. Ashida, H. Uekusa, F. Guo and K. D. M. Harris, *Chem. Commun.*, 2010, **46**, 4264–4266; (*b*) K. Fujii, H. Uekusa, N. Itoda, G. Hasegawa, E. Yonemochi, K. Terada, Z. Pan and K. D. M. Harris, *J. Phys. Chem. C*, 2010, **114**, 580–586; (*c*) K. Fujii, H. Uekusa, N. Itoda, E. Yonemochi and K. Terada, *Cryst. Growth Des.*, 2012, **12**, 6165–6172; (*d*) K. Fujii, M. Aoki and H. Uekusa, *Cryst. Growth Des.*, 2013, **13**, 2060–2066.

11 (*a*) A. L. Balch, *Gold Bull.*, 2004, **37**, 45–50; (*b*) P. Pyykko, *Angew. Chem., Int. Ed.*, 2004, **43**, 4412–4456; (*c*) V. W. Yam and E. C. Cheng, *Chem. Soc. Rev.*, 2008, **37**, 1806–1813; (*d*) M. J. Katz, K. Sakai and D. B. Leznoff, *Chem. Soc. Rev.*, 2008, **37**, 1884–1895; (*e*) H. Schmidbaur and A. Schier, *Chem. Soc. Rev.*, 2008, **37**, 1931–1951; (*f*) X. He and V. W.-W. Yam, *Coord. Chem. Rev.*, 2011, **255**, 2111–2123; (*g*) H. Schmidbaur and A. Schier, *Chem. Soc. Rev.*, 2012, **41**, 370–412.

12 Actually, direct evidence of the aurophilic interaction of **1Y** has not been obtained even by EXAFS study measured at 4 K. The peak assignable to the Au···Au distance of **1Y** was found around at 5 Å, which corresponded to the Au···Au distance of unground **1B**. This result may be caused by only the small amount of aurophilic interactions in **1Y**, so

that even EXAFS studies could not observe the aurophilic interactions. A more detailed discussion will be reported elsewhere.

13 Addition of other solvents, such as dichloromethane, chloroform, cyclohexanone and dimethoxyethane, induces various emission color changes of **2**. For example, chloroform addition to **2G** provided a red-emitting powder which shows emission spectrum peaked at 645 nm. Unfortunately, we can not determine, at present, detailed molecular arrangements of the resulting materials, and thus these behaviors will be discussed elsewhere. Moreover, recrystallization of **2** from cyclohexanone, THF, and dimethoxyethane (maximum solubility c_{max} > 0.1 mg mL^{-1}) afforded a yellow-emitting solid (similar to **2Y**). Since **2** can not solvate these solvents, it is proposed that non-solvated **2Y** was formed under these conditions.

14 **2Y** is also transformed to **2B** upon addition of acetone.

15 (*a*) J. Bernstein, *Polymorphism in molecular crystals*, Clarendon Press/International Union of Crystallography, 2002, vol. 14; (*b*) Y. Mnyukh, *Fundamentals of Solid-State Phase Transitions: Ferromagnetism and Ferroelectricity*, Authorhouse, 2001.

16 Residual electron density in 1-D channel is estimated to be seventeen electrons per unit cell. This is corresponding to 0.5 equivalents for acetone and/or 2 equivalents for water. ^{1}H NMR spectrum of **2G** confirms that both acetone and H_2O could be present (Fig. S12†).

17 D. Yan, G. Fan, Y. Guan, Q. Meng, C. Li and J. Wang, *Phys. Chem. Chem. Phys.*, 2013, **15**, 19845–19852.

18 A diffraction peak at 6.6° is derived from the residual **2G** phase contaminated within the **2Y** phase (see also Fig. S7c†).

19 For an example of PXRD measurements and the Rietveld refinement technique for the study of the crystalline size of the ground phase of mechanochromic compounds rather than full structure analysis, see: S. Perruchas, X. F. Le Goff, S. Maron, I. Maurin, F. Guillen, A. Garcia, T. Gacoin and J. P. Boilot, *J. Am. Chem. Soc.*, 2010, **132**, 10967–10969.

20 The **2Y** phase thermally transformed from **2G** can not further transform to the **2O** phase upon phase transition; whereas mechanically prepared **2Y** shows transformation into the **2O** phase. This result indicates that the preparation method of the **2Y** phase affects its phase transition behavior.

21 As mentioned above, no solvent molecules exist in the crystalline lattice of **2Y** based on thermal analyses, elemental analyses and ^{1}H NMR and IR spectroscopy (Fig. 8, S13 and S17 and Table S4†).

22 DSC analysis of **2B** was not performed because it is unstable without acetone.

23 This discussion agrees well with the fact that the as-synthesized form of **2** is principally similar to **2Y** as shown in the PXRD pattern (Fig. S6†), likely because a metastable form of **2Y** is kinetically trapped.